

Poststack Seismic Data Preconditioning via Dynamic Guided Learning

Javier Torres-Quintero*, Paul Goyes-Peñafiel*, Ana Mantilla-Dulcey†, Luis Rodríguez-López*, José Sanabria-Gómez†, Henry Arguello*

ABSTRACT

Seismic data preconditioning is essential for subsurface interpretation. It enhances signal quality while attenuating noise, improving the accuracy of geophysical tasks that would otherwise be biased by noise. Although classical poststack seismic data enhancement methods can effectively reduce noise, they rely on predefined statistical distributions, which often fail to capture the complexity of seismic noise. On the other hand, deep learning methods offer an alternative but require large and diverse data sets. Typically, static databases are used for training, introducing domain bias, and limiting adaptability to new noise poststack patterns. This work proposes a novel two-process dynamic training method to overcome these limitations. Our method uses a dynamic database that continuously generates clean and noisy patches during training to guide the learning of a supervised enhancement network. This dynamic-guided learning workflow significantly improves generalization by introducing variability into the training data. In addition, we employ a domain adaptation via a neural style transfer strategy to address the potential challenge of encountering unknown noise domains caused by specific geological configurations. Experimental results demonstrate that our method outperforms state-of-the-art solutions on both synthetic and field data, within and outside the training domain, eliminating reliance on known statistical distributions and enhancing adaptability across diverse data sets of poststack data.

INTRODUCTION

Seismic data preconditioning is crucial in preparing post-stack seismic data for geophysical downstream tasks, particularly subsurface interpretation (Chopra and Marfurt, 2013). It enables geologists to analyze subsurface structures with greater accuracy in tasks such as fault detection (Wei et al., 2022) and seismic attribute computation (Oumarou et al., 2021), facilitating the identification of promising areas for the exploration of mineral deposits, hydrocarbons, and geothermal resources (Gao et al., 2021; Malehmir et al., 2021). This process involves denoising and enhancing the signal quality, which becomes essential due to the nature of the seismic acquisition, as the acquired data is usually corrupted by noise, which increases the complexity of interpretation tasks.

Seismic noise has been studied and classified in the state-of-the-art into random noise (non-signal-dependent) and coherent noise (signal-dependent). Random noise is related to artifacts produced by environmental and equipment-related factors. This category includes noises such as spike-like noise in the seismic marine acquisition, which is characterized by intermittent, impulse-like disturbances. These are typically associated with large marine fauna, such as tuna, that occasionally interfere with the receivers (Hlebnikov et al., 2021); cross-feed noise, which is caused by faulty sensors and resembles noise in the form of stripe-like traces (Hlebnikov et al., 2021). Coherent noise is associated with the corruption of the signal during the data processing stage (Mrigya et al., 2023; Yang et al., 2023), it includes smile and frown artifacts produced by over-migration and under-migration of the data, respectively, and are linked to wave propagation phenomena (Yoo and Zwartjes, 2022); ground roll, which is a common coherent noise in land field seismic data it is a Rayleigh-type surface wave that masks relevant seismic events (Jia et al., 2024). An analysis of these types of noise reveals that seismic data is inherently corrupted. As coherent noise is associated with wave propagation, it could be misinterpreted as relevant signals even though coherent noise poses a greater risk to the accuracy of geophysical analysis during inter-

*Universidad Industrial de Santander, Department of Computer Science, Colombia. E-mail: javier.torres.quintero@hotmail.com, goyes.yesid@gmail.com, luis2238326@correo.uis.edu.co, henarfu@uis.edu.co. †Universidad Industrial de Santander, Department of Physics, Colombia. E-mail: ana.mantilla@correo.uis.edu.co, jsanabri@uis.edu.co.

pretation. The literature on denoising predominantly focuses on random noise, as it is more manageable to attenuate due to its consistency with known statistical distributions (Gao et al., 2024; Liu et al., 2024; Zhang et al., 2024; Wang et al., 2025). However, these distributions fail to capture the full complexity of seismic data, which can vary significantly based on site geology, data acquisition methods, and processing techniques. This bias in state-of-the-art denoising solutions highlights an opportunity to address noise outside these known distributions, enabling more accurate representations of seismic noise complexity.

A practical approach to handling high-complexity noises involves building representations that emulate field noise behavior, enabling its subtraction to obtain a clean sample. Image processing techniques create these representations by analytically defining noise as degradation models that corrupt clean data (Yoo and Zwartjes, 2022). This approach is commonly employed to address noise in post-stack seismic data (Yoo and Zwartjes, 2022; Wu et al., 2022; Mrigya et al., 2023).

Several methods have been developed in the literature based on noise emulation to enhance the quality of the poststack seismic data, from filters such as median and band-pass to state-of-the-art deep learning-based solutions. However, classic methods such as frequency-dependent noise attenuation (Al-Heety and Thabit, 2022) and structurally oriented coherent noise filtering (Dorn, 2018) depend on known distributions and established models like Gaussian. These approaches assume that seismic noise behaves similarly to these mathematical models, which could work to some extent. However, the complexity of seismic noise often goes beyond these models due to the number of variables involved in acquiring and processing seismic data (Kumar and Ahmed, 2021).

Deep learning-based solutions have shown significant improvements in handling diverse representations of seismic noise for denoising, often relying on supervised learning. This approach trains a denoising network using pairs of clean and noisy patches (Mrigya et al., 2023; Ren et al., 2022). Nonetheless, these solutions also present a disadvantage: Deep learning (DL) is data-driven, which implies that the method’s performance depends on the amount and distribution of the training data. Typically, a static database is used (Gao et al., 2024; Ren et al., 2022; Mrigya et al., 2023), where the data remains unchanged during training. On the other hand, unsupervised and self-supervised learning approaches, such as Deep Image Prior (DIP) or internal learning, have been explored to train enhancement networks without relying on external data (Qian et al., 2024; Wang et al., 2024). DIP and internal learning only depend on incomplete measurements to enhance seismic data. However, these methods often struggle with generalization because they require training for each specific data set. In the case of DIP, it is also necessary to know the degradation model or mask that affects the image (Ulyanov et al., 2020). Therefore, the main limitations are as follows: For classic methods, the dependence on math-

ematical models that fail to represent the complexity of field noise. For DL solutions, large and variable training data is required, and the static database limits the learning domain, leading to poor generalization across multiple data sets.

This work proposes an approach that improves generalization by adding variability to the database during training. This ensures the method is non-dependent on specific known distributions while avoiding using external data sets, often limited by data ownership in the industry. Our novel approach exploits the advantages of data augmentation to increase the diversity of traditional training databases.

The proposed method consists of two key processes: The dynamic database, which integrates a Generative Adversarial Network (GAN), and a degradation model to generate clean and corrupted poststack seismic patches, respectively, facilitating data augmentation through the application of the degradation model. The dynamic database guides the supervised enhancement task learning. In addition, to address the possibility of the network encountering unknown noise specific to a geological configuration, we employ domain adaptation via neural style transfer, as described by Du et al. (2022). This approach allows the model to adapt to new noise patterns beyond the training domain while retaining previously acquired knowledge.

To summarize, our main contributions are as follows:

1. We propose a supervised preconditioning method for poststack seismic data, leveraging a dynamic guided learning workflow. This method employs a high-variability training strategy based on dynamic data augmentation, enhancing the generalization capabilities of the network to unseen data with diverse noise characteristics.
2. We introduce a dynamic guided learning scheme with domain adaptation to handle new noise patterns effectively. The method minimizes the mismatch between test and training domains by utilizing a neural style transfer strategy to extract new noise patterns. This approach ensures independence from prior noise distributions and facilitates rapid fine-tuning to adapt to new geological conditions.
3. We validate the proposed method on synthetic and field seismic data, benchmarking its performance against classic and DL solutions. The results demonstrate that our approach consistently outperforms state-of-the-art methods by effectively capturing complex geological structures and adapting to diverse noise conditions, highlighting its superior robustness and accuracy.

DYNAMIC GUIDED LEARNING

Unlike the classic supervised approach, which relies on a static database with a fixed number of images and labels, the dynamic guided learning approach introduces variability. This allows for a more flexible training strategy. Dy-

dynamic guided learning consists of two processes, described in the following subsections: the dynamic database (I) and the supervised enhancement task (II) in a workflow shown in Figure 1. The first process involves generating clean patches using a generative model, denoted as $\mathbf{X} \in \mathbb{R}^{M \times N}$, where M corresponds to the time/depth samples and N represents the trace number. Noisy patches \mathbf{Y} are then created by applying a degradation model to the generated clean patches \mathbf{X} . This degradation step acts as a form of data augmentation and constitutes the dynamic database. The second process, the supervised enhancement task, is trained using the dynamically generated data from the database, guiding the learning of the task. Moreover, this workflow operates in cycles, where the dynamic database generates new training data on the CPU while the enhancement network is trained on the GPU. A cycle begins with data synthesis and ends when a predefined number of epochs is completed. These parallel processes ensure maximum efficiency in training by utilizing only the available GPU for model training while data generation occupies the CPU.

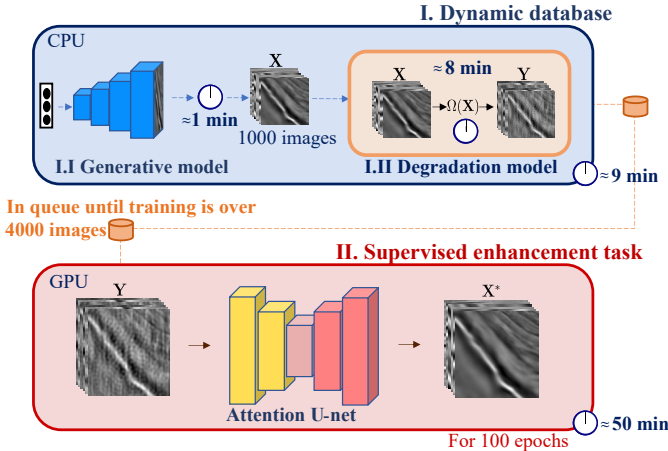


Figure 1: The dynamic guided learning workflow with two main processes: (I) the dynamic database that generates \mathbf{X} poststack seismic data using the generative model (1000 patches) and \mathbf{Y} noisy poststack seismic data (4000 patches) using the degradation model containing 12 different types of noise. (II) The supervised enhancement task learns distinctive features of poststack seismic data during training. While process (II) is training, process (I) generates the next batch of images with different types of noise randomly selected, completing one cycle, with (I) in CPU and (II) in GPU to maximize computational efficiency.

The proposed method focuses on learning the representation of local signal structures and scale-variable seismic noise patterns through a dynamic database, overcoming the limitations of deep learning-based seismic enhancement methods. This improves the generalization capability by feeding the enhancement network with diverse images, as explained in the following subsections.

Dynamic database

The first process of the proposed method consists of two components: a generative and a degradation model.

Generative model

To identify the most suitable generative model in terms of computational efficiency and generation quality, we evaluated the Fréchet Inception Distance (FID) metric and generation time on a CPU for the following approaches, as shown in Table 1: Variational Autoencoder GAN (VAE/GAN) (Larsen et al., 2016), Vector Quantized Variational Autoencoder (VQ-VAE) Van Den Oord et al. (2017), Wasserstein GAN (WGAN) (Arjovsky et al., 2017) and the Progressive Growing GAN (PGGAN) (Karras et al., 2018). It is important to note that we prioritized a balance between computational efficiency and the quality of generated samples. Given that GAN-based models satisfy these criteria, we focus our analysis on this class of models.

Table 1: Comparison of poststack seismic data generation quality, evaluating different models based on their FID scores and computational efficiency in terms of generation time on CPU. Bold numbers are the best performance while underlined numbers are the second best.

Model	\uparrow IS	\downarrow FID	\downarrow MMD	Time (s)
VAE/GAN	1.148	58.244	1.131	12
VQ-VAE	1.000	<u>19.027</u>	0.090	1200
WGAN-GP	1.004	60.738	0.054	152
PGGAN	1.201	10.250	<u>0.300</u>	<u>65</u>

The selected model was PGGAN as it achieved the best performance in the FID and IS metrics. Although PGGAN did not achieve the best performance in the MMD metric, it remained within a range close to zero. This result suggests that PGGAN exhibits high variability in synthesizing poststack seismic images. Therefore, while the numerical outcome is not the best, it is the second best in the MMD metric, indicating that the generated patches remain well-aligned with the post-stack seismic training distribution.

The generative neural network model \mathcal{G} , employs a network that learns the distribution of training data, starting from a low resolution of $K \times L$. It progressively adds layers until the required resolution $M \times N$ is achieved, where $M > K$ and $N > L$. The model is conditioned on a fixed normal distribution of latent vectors $\mathbf{z} \sim \mathcal{N}(0, \mathbf{I})$ where \mathbf{I} is an identity matrix, enabling the trained model to produce \mathbf{X} :

$$\mathbf{X} = \mathcal{G}(\mathbf{z}). \quad (1)$$

Figure 2 shows the generated clean poststack seismic patches coherent with field seismic scenarios based on the expertise of the authors with geology-based knowledge and the evaluated metrics.

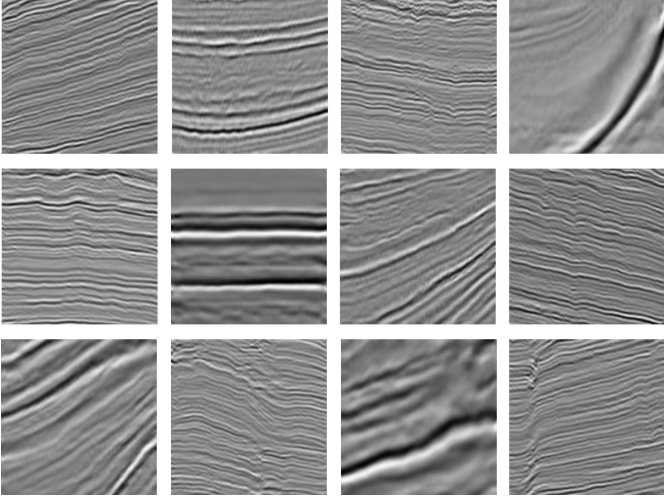


Figure 2: Examples of generated clean 128×128 poststack seismic patches.

Degradation model

To generate the inputs \mathbf{Y} of the supervised enhancement task, we employ a degradation model that can be mathematically described as follows:

$$\mathbf{Y} = \Omega(\mathbf{X}), \quad (2)$$

where $\Omega(\cdot)$ denotes an operator that corrupts the post-stack seismic data with 12 types of noise shown in Table 2. Each type of noise was identified by analyzing open-access field poststack seismic data, such as Kerry 3D (Minerals, 1995), Blake Ridge Hydrates 3D (Holbrook, 2015), and F3 Netherlands (Baroni et al., 2018). Based on the authors’ geophysical expertise, the most common noise types were categorized into 12 main types, with new noise patterns emerging from their combinations. Image processing techniques were employed to emulate these types of noise, as illustrated in Figure 3, which shows corrupted poststack seismic data with the characterized noises.

Each type of noise has a range of weights that varies depending on the implementation. For instance, in the case of Gaussian noise, it is the intensity and goes from 0, representing no noise, to 1, indicating the presence of only noise. In the case of linear noise, the parameter corresponds to the number of lines, ranging from 0, indicating no damage, to the full horizontal extent of the data, where no seismic feature is preserved. These weights allow data augmentation over the generated \mathbf{X} patches, as the model output is a tensor $\mathbf{Y} \in \mathbb{R}^{M \times N \times D}$, where D indicates the number of degradations randomly applied of corrupted patches, each with one randomly selected type of noise, and a combination of multiples noises in the last position. Figure 1 presents an example of this data augmentation, where 1000 poststack seismic patches are generated, and D is set to 4, increasing the data set to 4000 noisy patches.

The dynamic database is used to guide the learning of the supervised enhancement task.

Table 2: Characterization of 12 types of noise related to poststack seismic data, their categorization as coherent or random, and their causes.

Noise	Category	Cause
Gaussian	Random	Human related
Poison	Random	Human related
Speckle	Random	Human related
Salt and pepper	Random	Human related
Linear	Random	Cross-feed
Stripes	Random	Cross-feed
Blur	Random	Processing
Waves	Coherent	Smile and artifacts
Correlated g_1	Coherent	Footprint
Correlated g_2	Random	Spike-like
Correlated g_{12}	Coherent	Footprint
g_{12} blur	Random	Background

Supervised enhancement task

The supervised enhancement task employs a supervised learning approach with pairs of \mathbf{X} and \mathbf{Y} to train an enhancement network \mathcal{M}_θ to optimize the parameters θ by minimizing the loss function:

$$\theta^* = \underset{\theta}{\operatorname{argmin}} \mathcal{L}(\theta), \quad (3)$$

where \mathcal{L} is the cost function described in Equation 4.

The \mathbf{X} and \mathbf{Y} are generated dynamically. This process is performed recurrently, with the dynamic database preparing a new training batch for every defined number of epochs. This exposes \mathcal{M}_θ to different sets of noisy patches. The key advantage of this approach is that it increases the variability and adaptability of the training process.

Enhancement loss function

The loss function employed in this work is inspired by methodologies from related studies on seismic data enhancement (Goyes-Peñañel et al., 2024). It measures the similarity between the original clean seismic data \mathbf{X} , as defined in Equation 1, and the enhanced data $\mathbf{X}^* = \mathcal{M}_\theta(\mathbf{Y})$. Here, \mathbf{Y} represents the forward-transformed version of \mathbf{X} , obtained using the degradation model $\Omega(\cdot)$, as described in Equation 2. To capture this similarity, the loss function combines the Mean Absolute Error (MAE) and the Structural Similarity Index Measure (SSIM), striking a balance between pixel-level fidelity and perceptual image quality. The loss function is defined as:

$$\mathcal{L}(\theta) = \frac{1}{B} \|\mathbf{X} - \mathbf{X}^*\|_1 + (1 - \operatorname{SSIM}(\mathbf{X}, \mathbf{X}^*)), \quad (4)$$

where the first term, $\|\cdot\|_1$, represents the ℓ_1 -norm, which, when divided by B the batch size, results in the MAE, which evaluates the average absolute difference between

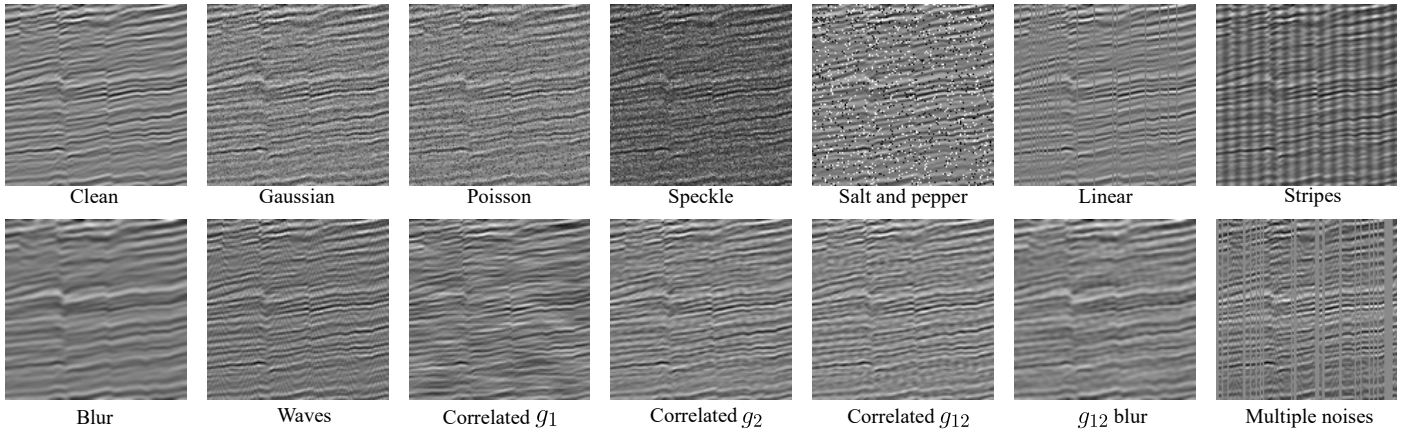


Figure 3: Visual example of a clean patch corrupted by the 12 type of noise described in Table 2. Note that multiple noise refers to a random combination of three types of noise.

the clean seismic data \mathbf{X} and the enhanced data \mathbf{X}^* . The second term involves the SSIM, which quantifies luminance, contrast, and structural similarity between \mathbf{X} and \mathbf{X}^* . It has a maximum value of 1, encouraging the enhancement to maintain perceptual consistency (Bakurov et al., 2022).

Enhancement network configuration

The supervised enhancement task uses a 2D U-net with attention blocks (Oktay et al., 2018). Downsampling and upsampling operations are performed using layers with 2×2 strides, respectively. Skip connections are included between the encoder and the decoder to facilitate the fusion of low-level and high-level features. Before the attention blocks, the input and output of the Attention U-net are concatenated to enhance the spatial information. Batch normalization and the ReLU activation function ensure consistency across all layers. The four attention blocks in the image enhancement process gradually improve the patch quality before reaching a convolutional layer with a single filter and a sigmoid activation function, which generates the enhanced seismic patch. The total number of trainable parameters is 34,877,421. Further details of the implementation can be found in the project’s repository.

Domain adaptation via neural style transfer

The performance of deep supervised learning models during testing is often lower than during the training phase due to biases introduced by the training data domain. This leads to a mismatch between the training and testing domains, as illustrated in Figure 5. Therefore, the network \mathcal{M}_θ must be adapted to the new domain. Training from scratch can effectively learn domain-specific features; however, this approach is highly inefficient, especially when dealing with multiple seismic data sets with distinct conditions, such as geological structures, acquisi-

tion instruments, or processing methods. Instead, we use a fine-tuning strategy that leverages pre-trained knowledge to adapt the network and learn new seismic features efficiently. To this end, we use an approach for generating field noise data using neural style transfer (Gatys et al., 2016). As Figure 4 shows, if the enhancement after inference (I) is unsatisfactory, this approach can incorporate the new noise pattern into the degradation model (II.II) as a complement of the 12 characterized types of noise to fine-tune the network following the same workflow as training. The new noise pattern is introduced by extracting the style from the field noisy poststack seismic data \mathbf{Y} and adapting it to the content data clean patches \mathbf{X} by synthesizing new data $\hat{\mathbf{Y}}$, initialized as \mathbf{X} , under the assumption that style features are noise features, using a pre-trained VGG-19 model. This improves generalization and helps resolve the domain mismatch problem. Figure 6 shows an example of the style transfer between a clean poststack seismic patch \mathbf{X} and field data \mathbf{Y} . The cost function for the optimization problem is expressed as follows:

$$\mathcal{L}_{total} = \alpha \mathcal{L}_c(\mathbf{X}, \hat{\mathbf{Y}}, l_c) + \beta \mathcal{L}_s(\mathbf{Y}, \hat{\mathbf{Y}}, l_s), \quad (5)$$

where \mathcal{L}_c is the content loss, calculated over the layer l_c , to preserve seismic information between \mathbf{X} and $\hat{\mathbf{Y}}$. Similarly, \mathcal{L}_s is the style loss calculated over the layer l_s , to extract the noise from the field image. Noise features are assumed to correspond to style features, derived from the calculation of Gram matrices for both the style and content data; α and β are the weights that determine the importance of structure \mathcal{L}_c and style \mathcal{L}_s , relative to each other.

EXPERIMENTS AND RESULTS

Data sets

The following synthetic and field open-access data sets were used for training: SEAM Phase 1 (Fehler and Keliher,

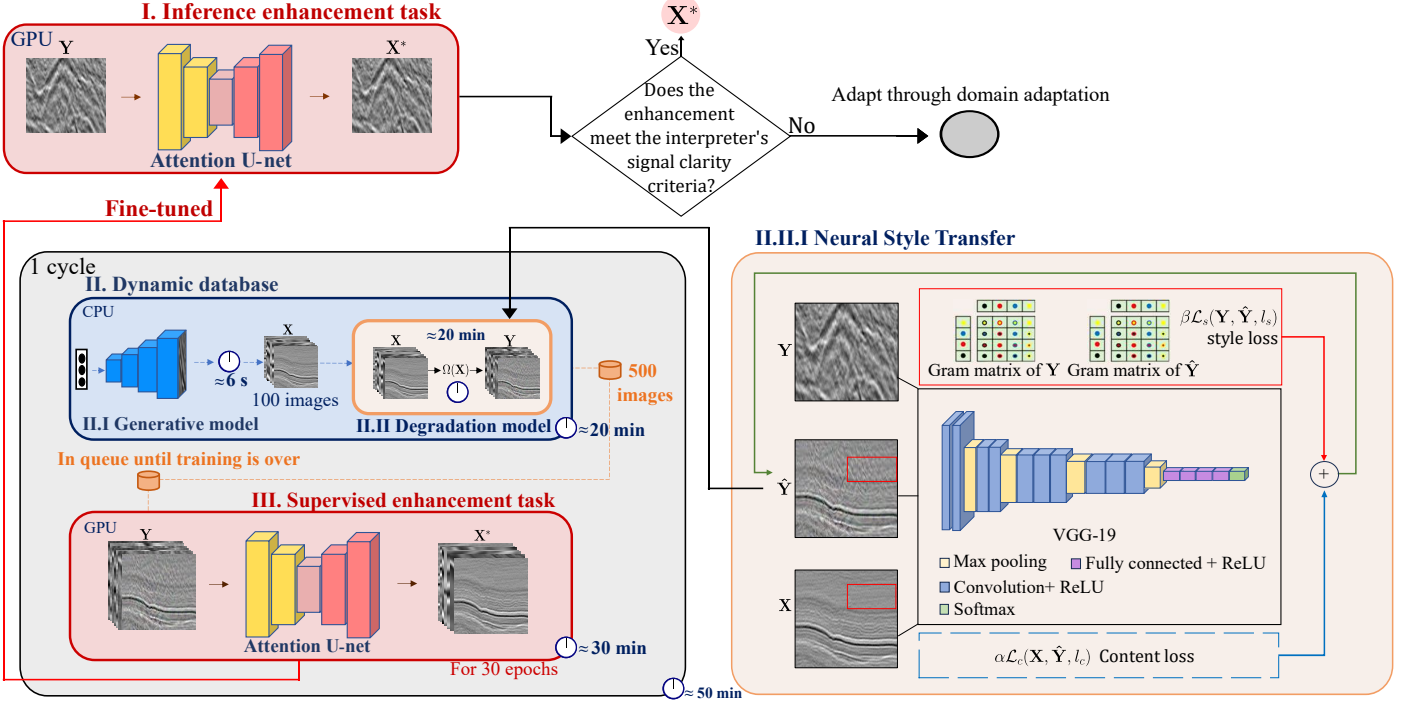


Figure 4: Domain adaptation via neural style transfer. When the inference enhancement task (I) testing does not meet enhancement criteria, the proposed method is employed to fine-tune the Attention U-net and adapt to the unknown noisy domain. The neural style transfer (number II.II.I) is used to adapt the domain and acts as a complement of the degradation model (number II.II), corrupting the X clean poststack seismic patches with the aim for the network to learn the new domain.

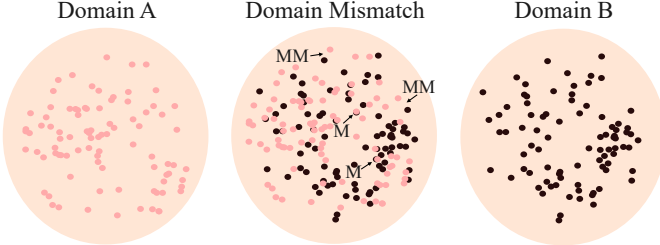


Figure 5: Example of domain mismatch across Domain A, which represents the training poststack seismic data, and Domain B, which represents the test field poststack seismic data. M stands for match, and MM for mismatch.

2011), TGS salt identification challenge (Howard et al., 2018), 1994 BP migration from topography (Sam and Kurt, 1995), AGL Elastic Marmousi (Martin et al., 2006), Kerry 3D (Minerals, 1995), and F3 Netherlands (Baroni et al., 2018). Patches with dimensions $M = 128$ and $N = 128$ were extracted from each data set, ensuring the selection of noise-free patches. Table 3 shows the number of patches extracted from each data set.

Metrics

To evaluate the performance of the PGGAN for data generation, state-of-the-art metrics, such as the inception score (IS), Fréchet inception distance (FID), and Maxi-

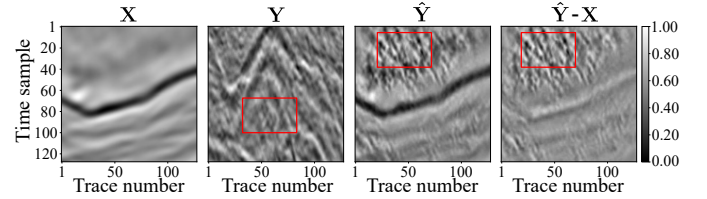


Figure 6: Domain adaptation on a clean poststack seismic patch X derived from a field noisy patch of the Kerry 3D data set Y . The generated data \hat{Y} with the content data's structure and the style data's noise. The style difference between \hat{Y} and X . The red box highlights a noisy area of the field-style data and the noise transfer over the generated patch.

imum Mean Discrepancy Metric (MMD) metrics were used (Dash et al., 2024). The Peak Signal-to-Noise Ratio (PSNR) and SSIM (Bakurov et al., 2022) metrics were employed to evaluate the enhancement over noisy poststack seismic data.

Experimental setup

The PGGAN model was trained for 770 epochs, following the implementation by Persson (2021), using the synthetic and field data sets presented in Table 3. The enhancement network, \mathcal{M}_θ , was trained for 15 cycles, each

Table 3: Number of field and synthetic patches for each data set.

Data set	Type	Number of patches
SEAM Phase 1	Synthetic	1119
TGS	Synthetic	630
1994 BP	Synthetic	803
AGL Elastic Marmousi	Synthetic	152
Kerry 3D	Field	3127
F3 Netherlands	Field	2134
Total		8000

consisting of 100 epochs. During training, in the dynamic database, the generative model generated 1000 \mathbf{X} post-stack data. The degradation model was used to augment the data with a factor of $D = 4$, resulting in a total of 4000 pairs of clean and corrupted patches, which were processed by \mathcal{M}_θ in each training cycle. By the end of training, \mathcal{M}_θ had learned from 60,000 unique patches. This total was derived from the product of the number of cycles (15) and the number of patches per cycle (4000). The total number of epochs across all training cycles was 1500. During testing, we found that this configuration of generated patches and the chosen degradation factor D yielded optimal performance. While this approach can be extended to a greater D factor or a larger number of generated patches, its selection was constrained by computational limitations. The Adam optimizer (Kingma and Ba, 2015) was employed, with a batch size of $B = 200$ and a learning rate set to 10^{-2} , subjected to an exponential decay of 0.6 every 200 epochs. The neural models were implemented using the PyTorch library. The **training equipment** was a system with an AMD Ryzen 7 5800X3D CPU for managing the dynamic database and an NVIDIA GeForce RTX 4090 GPU for the supervised enhancement task. Under these settings, the training of the 15 cycles took 15 hours to complete, required 9 minutes to generate the 4000 patches, and 50 minutes for the 100 epochs of training per cycle. The style transfer loss weights for domain adaptation were set to $\alpha = 1$ and $\beta = 50$. The **testing equipment** consisted of an Intel(R) Core(TM) i7-10700K CPU and an NVIDIA GeForce RTX 3080 ti GPU to demonstrate computational efficiency.

To demonstrate the effectiveness of the proposed method, we conducted four experiments in local and complete post-stack seismic sections.

Experiment I

The enhancement network, trained using the dynamic guided learning workflow, was evaluated on 2D local post-stack seismic data with spatial dimensions of 128×128 . In this experiment, a clean seismic patch was corrupted using the 12 characterized types of noise to prove the en-

hancement efficiency over the known noise domain.

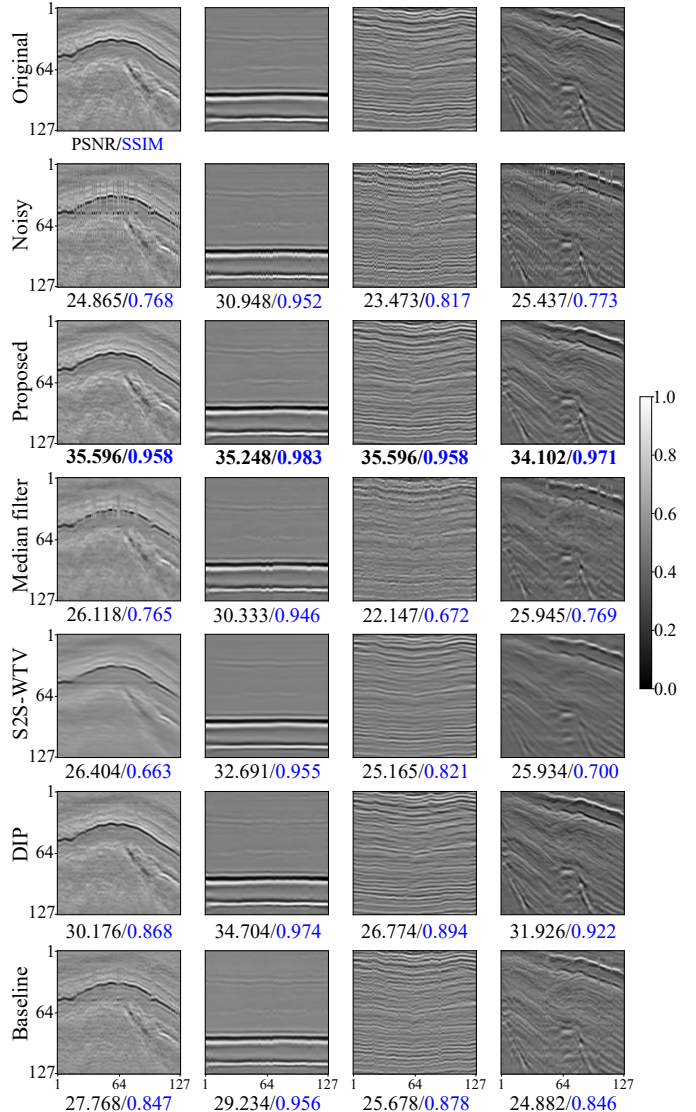


Figure 7: Clean-generated poststack seismic patches (original) corrupted (noisy) by linear noise, along with a comparison of the enhancement achieved using the proposed method and the state-of-the-art solutions, using PSNR (dB) and SSIM metrics. Bold numbers indicate the best result of the enhancement.

Three distinct noise weights, low, medium, and high, were assigned for each noise type. Each noise was applied 500 times for every weight, resulting in 1500 different instances of corrupted data per type of noise due to the stochastic nature of the noise generation process. The method’s performance was evaluated by calculating the average PSNR and SSIM metrics across the 1500 corrupted instances for each type of noise, taking an average enhancement time of 8 milliseconds per patch. We also compared the method with other state-of-the-art enhancement methods, such as the median filter, which attenuates noise by replacing each pixel value with the median of its neighboring pixels (George et al., 2018); self2self weighted total vari-

Table 4: Comparison metrics from experiment I. PSNR (dB) and SSIM metrics across different simulated types of noise for enhancement methods, including the median filter, DIP, S2S-WTV, and Baseline. Bold text indicates the best result, while underlined text highlights the second-best.

Noises	Medial filter		DIP		S2S-WTV		Baseline		Proposed	
	SSIM	PSNR	SSIM	PSNR	SSIM	PSNR	SSIM	PSNR	SSIM	PSNR
Gaussian	0.783	22.947	<u>0.965</u>	<u>31.992</u>	0.952	29.021	0.975	31.658	0.985	33.457
Poisson	0.784	22.899	<u>0.961</u>	<u>31.997</u>	0.952	28.493	0.974	31.291	0.986	34.248
Speckle	0.563	15.787	<u>0.908</u>	<u>27.273</u>	0.781	16.804	0.807	19.370	0.934	27.336
Salt and pepper	0.712	20.833	<u>0.881</u>	<u>28.028</u>	0.731	20.742	0.825	22.551	0.992	35.922
Linear	0.560	18.867	<u>0.947</u>	<u>29.238</u>	0.839	23.620	0.926	26.580	0.994	36.859
Waves	0.770	22.124	0.957	30.986	0.949	27.884	<u>0.976</u>	<u>31.602</u>	0.991	35.319
Stripes	0.633	18.838	<u>0.964</u>	<u>32.717</u>	0.798	20.687	0.948	25.201	0.998	39.361
Correlated g_1	0.782	22.774	0.944	<u>29.538</u>	0.934	27.272	<u>0.965</u>	29.442	0.972	31.108
Correlated g_2	0.784	22.923	0.950	<u>31.654</u>	0.942	28.509	<u>0.978</u>	31.001	0.987	34.262
Blur	0.516	17.400	0.904	30.426	0.550	17.707	0.600	19.085	<u>0.901</u>	<u>27.337</u>
Correlated g_{12}	0.796	23.124	<u>0.954</u>	<u>31.062</u>	0.953	28.775	0.981	31.271	0.984	33.593
g_{12} blur	0.683	19.403	<u>0.948</u>	<u>30.456</u>	0.770	20.496	0.851	22.129	0.981	31.543

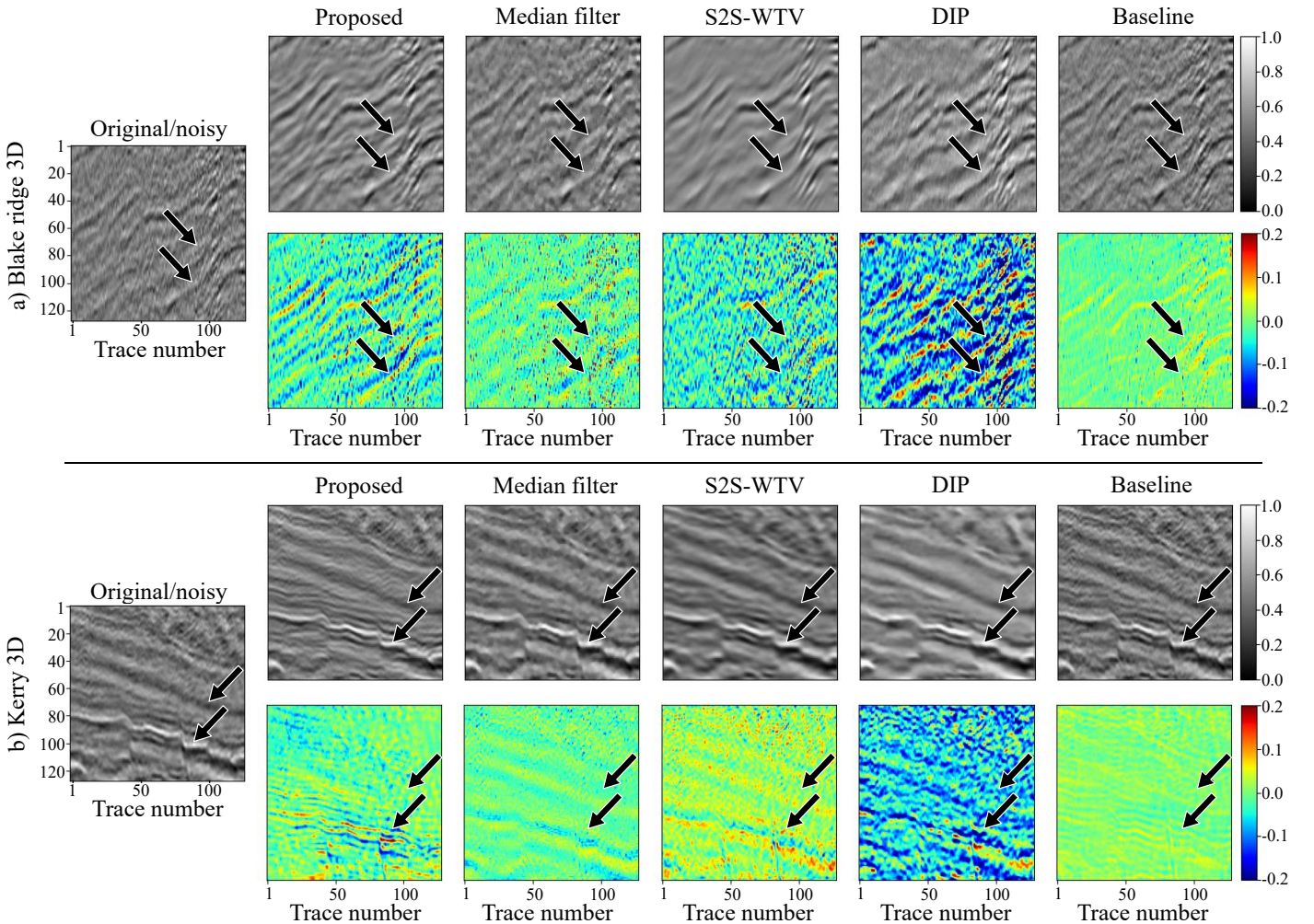


Figure 8: Visual results of experiment II. Local 128×128 patches from a) Blake Ridge 3D and b) Kerry 3D data sets enhanced compared against state-of-the-art methods and the difference between the original and enhanced data.

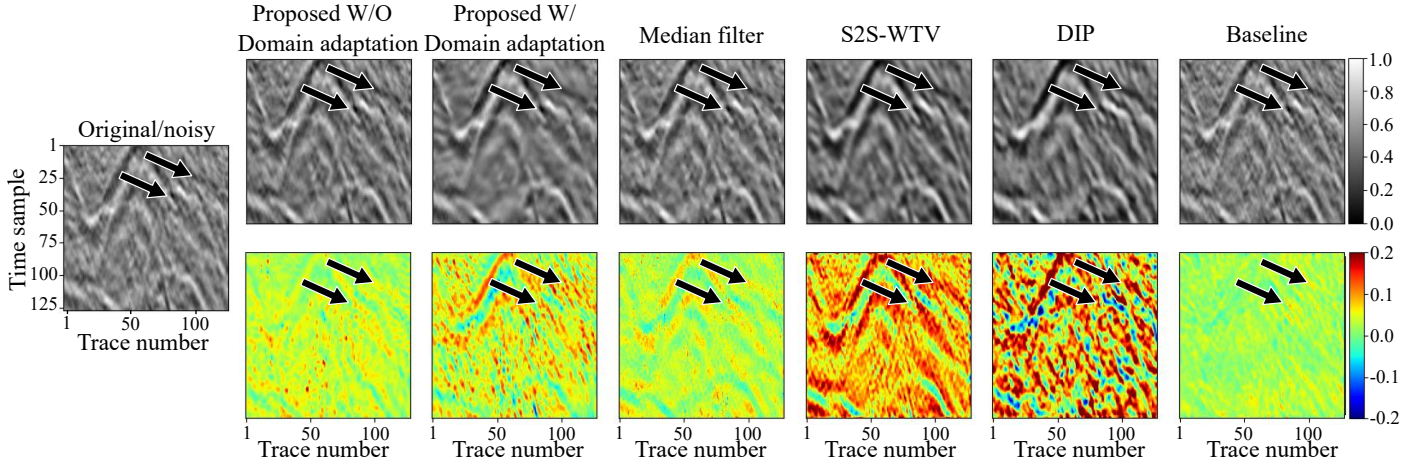


Figure 9: Visual results of experiment III. Local patches from the Kerry 3D data set enhanced with (W/) and without (W/O) domain adaptation compared against state-of-the-art methods and the difference between the original and enhanced data.

ation (S2S-WTV), which employs an optimization-based method to attenuate noisy signals (Xu et al., 2023); DIP (Ulyanov et al., 2020); and the baseline, which refers to the enhancement network of the proposed method trained using a classical supervised learning approach for 1500 epochs. The training process utilized a static database comprising clean and noisy patches, where the noisy patches were generated from the 12 characterized types of noise.

Figure 7 illustrates the process of corrupting a patch and the enhancement using the proposed method, demonstrating its advantage in preserving the signal integrity of seismic reflection interfaces, something that other methods, such as DIP and S2S-WTV, fail to achieve due to over-smoothing. In contrast, the baseline and median filter methods struggle with effective noise attenuation. Table 4 summarizes the results for all types of noise. This experiment shows that our method achieves an average improvement over the state-of-the-art solutions of up to 8 dB in PSNR and 0.127 in SSIM for noise attenuation across the characterized types of noise.

It is worth noting that even though the proposed method exhibited superior performance, it was outperformed only by DIP under Blur-type noise by 3 dB in PSNR, as shown in Table 4. This discrepancy may be attributed to DIP’s reliance on a noise mask, which assumes prior knowledge of noise characteristics. However, this represents an ideal scenario not met in real-world applications, as the noise in field poststack data is often unknown. Nonetheless, the proposed approach still achieved the second-best performance compared to the ideal case.

Experiment II

This experiment used 128×128 patches of 2D poststack seismic field data for testing. The ground truth for this data is unavailable, highlighting the method’s application in a field scenario. Figure 8 illustrates the experimental results on patches from the Kerry 3D and Blake Ridge 3D

data sets.

As shown in Figure 8, the patch from Blake Ridge 3D exhibits linear noise that affects the continuity of seismic events, while the patch from Kerry 3D contains a random-like noise resembling a Gaussian distribution. After training with the dynamic guided learning workflow, the enhancement network effectively improves the signal in local patches while preserving the coherence of seismic structures, outperforming comparable approaches such as DIP and S2S-WTV. While these methods occasionally yield good results, they often lead to over-smoothing of the seismic signal, as seen in the Blake Ridge patch. In contrast, the proposed approach avoids this issue, preserving the seismic reflection events highlighted by the black arrows in the Kerry and Blake Ridge patches. Notably, DIP struggles due to its reliance on a noise mask, which is typically unavailable in real-world applications. This underscores the proposed method’s ability to maintain structural integrity by distinguishing and highlighting distinct features of poststack seismic data, making it more reliable across diverse data sets.

Experiment III

Although training with the dynamic guided learning workflow effectively enhances seismic signals, there remains a possibility of encountering seismic data outside the training domain. The 12 characterized types of noise provide a robust representation of potential seismic noise scenarios. However, due to complex geological settings, they may not cover the full spectrum of possible seismic noise conditions. To address this issue, we employ domain adaptation using neural style transfer to learn new noise patterns.

In this experiment, the enhancement of a patch from the Kerry 3D data set containing a noise type unknown to the network was unsatisfactory. Consequently, we applied the domain adaptation strategy. Figure 9 illustrates the results with (W/) and without domain adaptation (W/O).

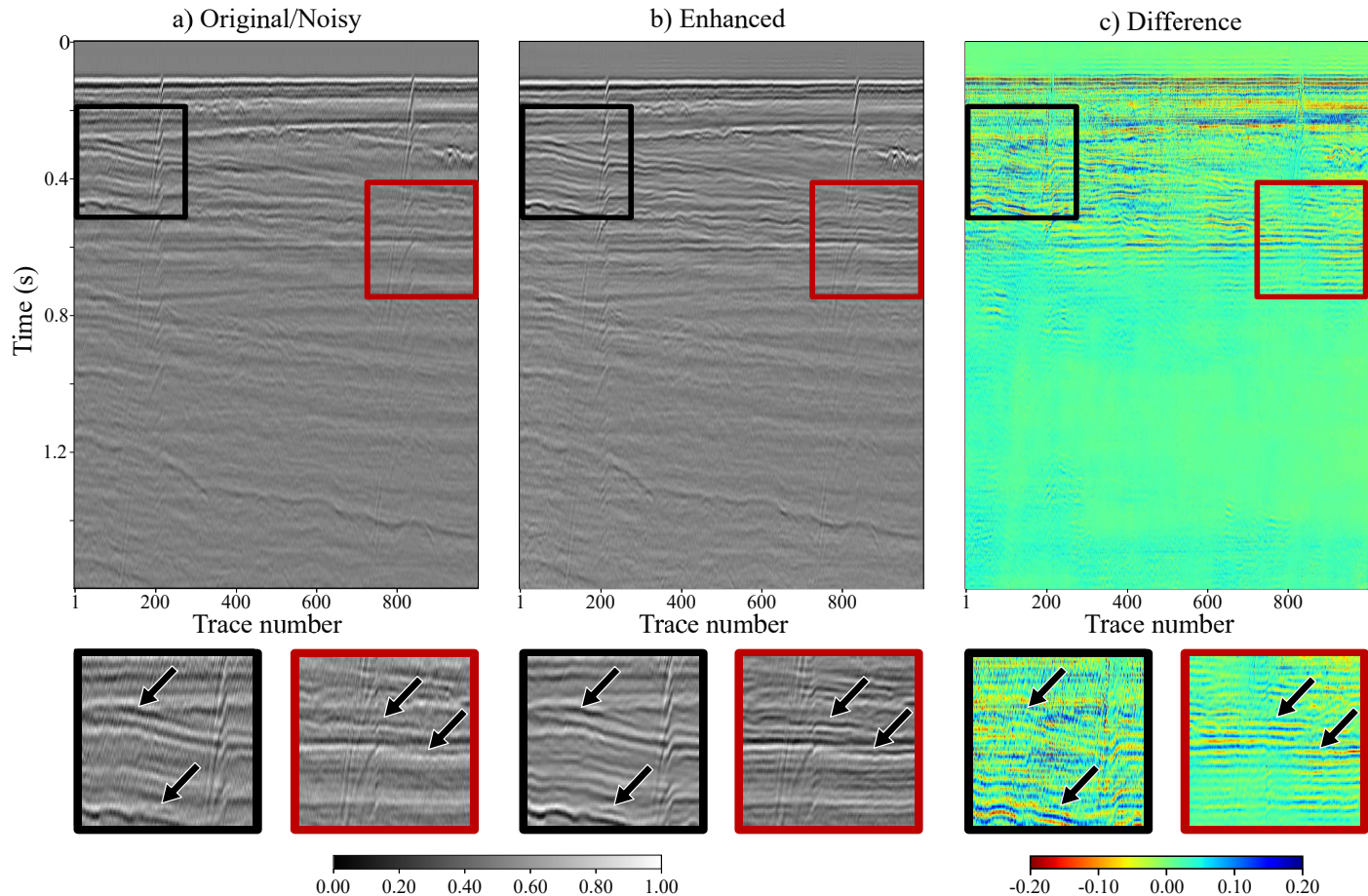


Figure 10: Visual results of experiment IV using the Mobil AVO Viking Graben data set. a) the original data with noise artifacts, (b) the enhanced complete section and c) the difference between a) and b). Zoomed-in views of regions black and red highlight the main enhancement features.

The W/ results were achieved by fine-tuning the network for 30 epochs. The black arrows highlight that while the proposed method successfully attenuates noise by focusing on the diagonal noise pattern after domain adaptation, S2S-WTV and DIP over-corrected some signals. In contrast, the median filter and baseline methods failed to reduce the noise level effectively.

Experiment IV

The results presented in the previous sections demonstrate that dynamic guided learning is effective for training the supervised enhancement task and outperforms state-of-the-art solutions. To evaluate the method’s applicability in field poststack seismic sections used in seismic processing workflows, we conducted tests over the Mobil AVO Viking Graben data set (Keys and Foster, 1994). It is worth noting that this data set was not used during training, emphasizing the robustness of the method’s generalization ability.

The enhancement network was trained using patches with spatial dimensions of 128×128 . To enhance poststack seismic sections exceeding the training dimensions, the sec-

tions were divided into patches that matched the training size, incorporating overlapping regions. Each patch was enhanced individually, and the enhanced data was reconstructed by taking the median of the overlapping regions. This approach was designed to preserve as many relevant signals as possible. The entire process, including patch division, enhancement, and reassembly of the seismic section for the Mobil AVO Viking Graben data set, took 18 seconds. This demonstrates that the method effectively enhances poststack seismic data and is computationally efficient. Figure 10 showcases the results, visually comparing the original noisy data and the enhanced version.

Figure 10a shows common artifacts in poststack seismic data, such as random high-frequency noise. The red box highlights a region with this particular noise pattern that masks structural details in the original data. Such noise degrades the visual quality of seismic images, affecting their analysis. Our method, illustrated in Figure 10b, effectively attenuates this noise, leading to more evident seismic reflections. The enhanced data further demonstrates improved continuity and better feature visibility over the black box. Notably, regions emphasized by black arrows across all boxes illustrate areas where significant

improvements have been achieved, enhancing the overall coherence of the complete section.

CONCLUSIONS

This work presents a robust and adaptable method for data preconditioning in seismic analysis. Given the significant variability of seismic noise across different geological settings, our approach provides a reliable solution for mitigating noise-related challenges, thereby enhancing the accuracy and reliability of seismic interpretation in industrial applications.

Our method demonstrates independence from specific seismic noise domains. Although the network was initially trained on 12 characterized types of noise, it could adapt during testing, effectively addressing field-specific and previously unknown noise domains that challenge the enhancement task. This adaptability underscores the method's applicability to synthetic and field data sets outside the training domain.

ACKNOWLEDGMENTS

This work was funded by the Vicerrectoría de Investigación y Extensión from Universidad Industrial de Santander under Project 3925. The authors acknowledge the High Dimensional Signal Processing Group (HDSP) from Universidad Industrial de Santander for providing the computational resources to run the experiments.

DATA AND MATERIALS AVAILABILITY

For reproducibility, the data and codes to replicate the proposed method are available at <https://github.com/TJaqui/Seismic-Denoising-Scheme>.

REFERENCES

- Al-Heety, A. J. R., and H. A. Thabit, 2022, Random and coherent noise attenuation for 2D land seismic reflection line acquired in Iraq: *Geophysical Prospecting*, 337–354.
- Arjovsky, M., S. Chintala, and L. Bottou, 2017, Wasserstein generative adversarial networks: *International conference on machine learning*, PMLR, 214–223.
- Bakurov, I., M. Buzzelli, R. Schettini, M. Castelli, and L. Vanneschi, 2022, Structural similarity index (SSIM) revisited: A data-driven approach: *Expert Systems with Applications*, **189**, 116087.
- Baroni, L., R. M. Silva, R. S. Ferreira, D. Chevitarese, D. Szwarcman, and E. Vital Brazil, 2018, Netherlands F3 interpretation dataset.
- Chopra, S., and K. J. Marfurt, 2013, Preconditioning seismic data with 5D interpolation for computing geometric attributes: *The Leading Edge*, **32**, 1456–1460.
- Dash, A., J. Ye, and G. Wang, 2024, A Review of Generative Adversarial Networks (GANs) and Its Applications in a Wide Variety of Disciplines: From Medical to Remote Sensing: *IEEE Access*, **12**, 18330–18357.
- Dorn, G. A., 2018, Structurally Oriented Coherent Noise Filtering: *First Break*, **36**, 37–45.
- Du, H., Y. An, Q. Ye, J. Guo, L. Liu, D. Zhu, C. Childs, J. Walsh, and R. Dong, 2022, Disentangling Noise Patterns From Seismic Images: *Noise Reduction and Style Transfer: IEEE Transactions on Geoscience and Remote Sensing*, **60**, 1–14.
- Fehler, M., and P. J. Keliher, 2011, SEAM Phase 1: Challenges of Subsalt Imaging in Tertiary Basins, with Emphasis on Deepwater Gulf of Mexico: *Society of Exploration Geophysicists*.
- Gao, K., L. Huang, and T. Cladouhos, 2021, Three-dimensional seismic characterization and imaging of the Soda Lake geothermal field: *Geothermics*, **90**, 101996.
- Gao, Z., H. Chen, Z. Li, and B. Ma, 2024, Multiscale Residual Convolution Neural Network for Seismic Data Denoising: *IEEE Geoscience and Remote Sensing Letters*, **21**, 1–5.
- Gatys, L. A., A. S. Ecker, and M. Bethge, 2016, Image Style Transfer Using Convolutional Neural Networks: *2016 IEEE Conference on Computer Vision and Pattern Recognition (CVPR)*, 2414–2423.
- George, G., R. M. Oommen, S. Shelly, S. S. Philipose, and A. M. Varghese, 2018, A Survey on Various Median Filtering Techniques For Removal of Impulse Noise From Digital Image: *2018 Conference on Emerging Devices and Smart Systems (ICEDSS)*, 235–238.
- Goyes-Peñañel, P., L. Suárez-Rodríguez, C. V. Correa, and H. Arguello, 2024, GAN-supervised Seismic Data Reconstruction: An Enhanced-Learning for Improved Generalization: *IEEE Transactions on Geoscience and Remote Sensing*.
- Hlebnikov, V., T. Elboth, V. Vinje, and L.-J. Gelius, 2021, Seismic denoising scheme for data acquisition in towed marine seismic: A tutorial: *GEOPHYSICS*, **86**, W1–W19.
- Holbrook, S., 2015, Project Blake Ridge Hydrates 3D.
- Howard, A., A. Sharma, A. Lenamond, J. Adamck, M. McDonald, S. Kainkaryam, and W. Cukierski, 2018, TGS Salt Identification Challenge.
- Jia, Z., W. Lu, M. Zhang, and Y. Miao, 2024, Ground-roll Separation From Land Seismic Records Based on Convolutional Neural Network.
- Karras, T., T. Aila, S. Laine, and J. Lehtinen, 2018, Progressive Growing of GANs for Improved Quality, Stability, and Variation: Presented at the International Conference on Learning Representations.
- Keys, R. G., and D. J. Foster, eds., 1994, Mobil avo viking graben line 12 data released for 1994 seg workshop: *Society of Exploration Geophysicists (SEG)*. SEG File Publications, No. No 4.
- Kingma, D., and J. Ba, 2015, Adam: A method for stochastic optimization: Presented at the International Conference on Learning Representations (ICLR).
- Kumar, D., and I. Ahmed, 2021, *1, in Seismic Noise: Springer International Publishing*, 1442–1447.
- Larsen, A. B. L., S. K. Sønderby, H. Larochelle, and O. Winther, 2016, Autoencoding beyond pixels using

- a learned similarity metric: International conference on machine learning, PMLR, 1558–1566.
- Liu, X., F. Lyu, L. Chen, C. Li, S. Zu, and B. Wang, 2024, Seismic Random Noise Suppression Based on Deep Image Prior and Total Variation: *IEEE Transactions on Geoscience and Remote Sensing*, **62**, 1–11.
- Malehmir, A., M. Markovic, P. Marsden, A. Gil, S. Buske, L. Sito, E. Bäckström, M. Sadeghi, and S. Luth, 2021, Sparse 3D reflection seismic survey for deep-targeting iron oxide deposits and their host rocks, Ludvika Mines, Sweden: *Solid Earth*, **12**, 483–502.
- Martin, G. S., R. Wiley, and K. J. Marfurt, 2006, Marmousi2: An elastic upgrade for marmousi: *The Leading Edge*, **25**, 156–166.
- Minerals, N. Z. C., 1995, Kerry 3D dataset.
- Mrigya, F., R. Samiran, F. Viviane, and H. Satyan Singh, 2023, A Comparative Analysis of Convolutional Neural Networks for Seismic Noise Attenuation: SPE EuroPEC - Europe Energy Conference featured at the 84th EAGE Annual Conference & Exhibition.
- Oktay, O., J. Schlemper, L. L. Folgoc, M. Lee, M. Heinrich, K. Misawa, K. Mori, S. McDonagh, N. Y. Hammerla, B. Kainz, B. Glocker, and D. Rueckert, 2018, Attention U-Net: Learning Where to Look for the Pancreas: Presented at the Medical Imaging with Deep Learning.
- Oumarou, S., D. Mabrouk, T. C. Tabod, J. Marcel, S. N. III, J. M. A. Essi, and J. Kamguia, 2021, Seismic attributes in reservoir characterization: an overview: *Arabian Journal of Geosciences*, **14**, 402.
- Persson, A., 2021, ProGAN implementation in PyTorch: <https://github.com/aladdinpersson/Machine-Learning-Collection/tree/master/ML/Pytorch/GANs/ProGAN>. (Accessed: 2024-11-16).
- Qian, F., H. Hua, Y. Wen, S. Pan, G. Zhang, and G. Hu, 2024, Unsupervised 3-D Seismic Erratic Noise Attenuation With Robust Tensor Deep Learning: *IEEE Transactions on Geoscience and Remote Sensing*, **62**, 1–16.
- Ren, H., X. Wen, and C. Tang, 2022, Denoising seismic data with drilling noise based on GAN: SEG 2021 Workshop: 4th International Workshop on Mathematical Geophysics: Traditional & Learning, Virtual, 17–19 December 2021, Society of Exploration Geophysicists, 126–128.
- Sam, G., and M. Kurt, 1995, Migration from topography: Improving the near-surface image.
- Ulyanov, D., A. Vedaldi, and V. Lempitsky, 2020, Deep Image Prior: *International Journal of Computer Vision*, **128**, 1867–1888.
- Van Den Oord, A., O. Vinyals, et al., 2017, Neural discrete representation learning: *Advances in neural information processing systems*, **30**.
- Wang, H., J. Lin, Y. Li, X. Dong, X. Tong, and S. Lu, 2024, Self-Supervised Pretraining Transformer for Seismic Data Denoising: *IEEE Transactions on Geoscience and Remote Sensing*, **62**, 1–25.
- Wang, X., Y. Sui, and J. Ma, 2025, Quadratic Unet for seismic random noise attenuation: *Geophysics*, **90**, V43–V55.
- Wei, X.-L., C.-X. Zhang, S.-W. Kim, K.-L. Jing, Y.-J. Wang, S. Xu, and Z.-Z. Xie, 2022, Seismic fault detection using convolutional neural networks with focal loss: *Computers & Geosciences*, **158**, 104968.
- Wu, H., B. Zhang, and N. Liu, 2022, Self-adaptive denoising net: Self-supervised learning for seismic migration artifacts and random noise attenuation: *Journal of Petroleum Science and Engineering*, **214**, 110431.
- Xu, Z., Y. Luo, B. Wu, and D. Meng, 2023, S2S-WTV: Seismic Data Noise Attenuation Using Weighted Total Variation Regularized Self-Supervised Learning: *IEEE Transactions on Geoscience and Remote Sensing*, **61**, 1–15.
- Yang, W., X. Chen, and Y. Rao, 2023, Seismic random noise attenuation using DnCNN with stratigraphic dip constraint: *Journal of Geophysics and Engineering*, **20**, 1172–1179.
- Yoo, J., and P. Zwartjes, 2022, Attenuation of seismic migration smile artifacts with deep learning: *Artificial Intelligence in Geosciences*, **3**, 123–131.
- Zhang, Y., C. Zhang, and L. Song, 2024, A two-stage seismic data denoising network based on deep learning: *Studia Geophysica et Geodaetica*.